The influence of particle properties on impact damage in LiF

In the course of a broad investigation of the mechanisms of solid particle erosion [1–3], the present authors have used a single-stage gas gun to conduct various impact experiments. In one series of experiments, spherical chrome steel spheres were fired perpendicularly against mechanically polished {1 0 0} surfaces of LiF monocrystals at velocities ranging from 50 to 350 m sec^{-1}; and in another series similar size WC–6% Co spheres were fired at similar targets under identical conditions. These experiments revealed several interesting differences in target response arising from the change in particle type. This note both reports these effects and suggests an explanation for their occurrence.

The steel spheres weighed 16.2 mg and had a diameter of 1.5875 mm and a Vickers Hardness Number (VHN) ~800 kg mm^{-2}; and the WC spheres weighed 30 ± 1 mg and had a diameter of 1.575 ± 0.025 mm and a VHN ~2000 kg mm^{-2} [1]. Examination of spent spheres of both kinds by surface profilometry and microscopy revealed no evidence of departure from sphericity due to plastic deformation during the impact event. In both series of experiments the targets were mechanically polished 10 mm × 10 mm × 5 mm slabs* prepared and mounted as described in [1].

The damage shown in Fig. 1 is typical of that produced by either kind of sphere over a wide range of velocities. It consists of a central crater, apparently formed by a combination of {1 1 0}⟨1 $\bar{1}$ 0⟩ glide and modes II and III cleavage crack propagation, and a surrounding region from which material has been lost through intersection of {1 0 0} and {1 1 0} cleavage cracks with one another and with the free surface. This latter region encroaches further into the central crater as the impact velocity is raised.

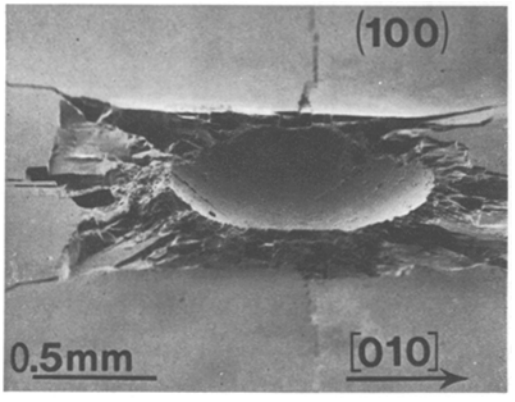

Figure 1 Scanning electron micrograph of the impact damage produced by a steel sphere with a velocity of 204 m sec^{-1} (70° tilt).

To characterize this damage quantitatively, two kinds of measurements were made. First, mass losses were determined gravimetrically; and then profilometer traces were made across each crater in ⟨100⟩ directions at 50 μm intervals. Crater depth l (relative to the original surface) and diameter (in the same plane) were determined directly from the deepest (diametral) trace in each case.

In addition, the impact process was modelled by considering a rigid sphere of radius r and mass m impinging normally on an ideal plastic-rigid half-space and assuming that the pressure over the area of contact is uniform and has a constant value p (the dynamic hardness) throughout the impact event [1]. Since this model implies that all of the particle kinetic energy is expended in permanently deforming the target,

$$pV = \tfrac{1}{2}mv_0^2, \tag{1}$$

where V is the crater volume and v_0 the impact velocity. Equation 1 can also be written as

$$p = \frac{mv_0^2}{2\pi l^2(r - l/3)}. \tag{2}$$

The mass loss data obtained from the two series of impacts are shown in Fig. 2; and superimposed on each set of data is a parabola of the form

$$m_l = kmv_0^2, \tag{3}$$

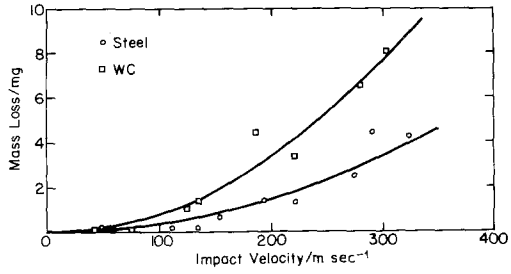

Figure 2 Variation of mass loss with impact velocity.

*Obtained from Harshaw Chemical Company, 6801 Cochran Road, Solon, Ohio 44139, USA, and containing as their principal impurities 100 to 200 ppm each of Ca and Fe.

0022–2461/79/123006–03$02.30/0

where m_1 is the mass loss and k the mass loss coefficient. This latter parameter, which is a measure of the "erosive efficiency" of unit mass of impacting particles, rises from 2.3×10^{-6} to 2.8×10^{-6} m^{-2} sec^2 when the steel spheres are replaced by those of WC.

Fig. 3 shows the corresponding dynamic hardness values calculated from the measured crater depths by means of Equation 2. A straight line representing the average of the individual values has been drawn through the data obtained from steel spheres, for the scatter in these data precludes identification of any clear velocity dependence of the dynamic hardness; but the curve fitted to the data from the experiments with WC spheres assumes a power function dependence of dynamic hardness on impact velocity. The remarkable feature of these results is that the dynamic hardness is independent of impact velocity and equal to 483 ± 59* kg mm^{-2} when steel particles are used, but decreases asymptotically with increasing impact velocity to less than half this value when WC particles are employed. It may be seen from these data that WC spheres produce larger craters and smaller dynamic hardnesses than do steel ones of the same kinetic energy.

It was also discovered from the accompanying surface profilometry measurements that post-impact elastic recovery of the target in general leads to a proportionally greater reduction in crater diameter than depth. The effect of such recovery is, therefore, to reduce the crater dimensions and increase the apparent dynamic hardness; but it is unlikely that the slight differences in the extent of such recovery-induced phenomena produced by WC as compared to steel spheres can account for the observed differences in dynamic hardness.

The differences in mass loss and dynamic hardness likewise cannot reasonably be attributed to the greater strain and lower strain-rate resulting from the slower deceleration of the more massive WC particles over a longer time and distance. One reason is that the differences in strain ($\lesssim 1.2\times$) and strain rate ($\sim 2\times$) involved are too small to alter the flow stress sufficiently to account for a factor $2\times$ in the dynamic hardness, and another is that decreasing the strain rate and increasing the strain have opposite effects on the flow and fracture of a semi-brittle solid such as LiF. Specifically, decreasing the strain rate tends to favour flow over fracture, whereas increasing the strain produces more blocked slip bands capable of nucleating cracks.

It therefore seems that the greater mass loss and dynamic hardness values produced by the WC spheres stem from their greater elastic mis-match with the target and their rougher surfaces (which should result in a higher coefficient of friction in the contact region). Since these factors presumably influence the present Boussinesq stress field in much the same manner as they affect the Hertzian stress field [4, 5], they will tend to increase the extent of the annular region around the contact area in which radial tensile stresses act and from which material is lost (Fig. 1). Hence, it is suggested that the greater material loss occurs because the increased size of the region in which tensile stresses act results in propagation of more surface flaws, and that this greater loss leads to a lower dynamic hardness by reducing the lateral elastic constraints on the process of crater formation.

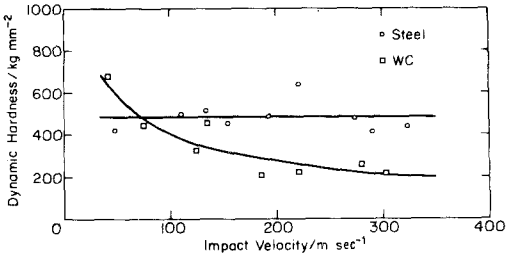

Figure 3 Variation of dynamic hardness with impact velocity.

*± one standard deviation.

Acknowledgement

Work supported jointly by the US Army Research Office under Grant no. DAAG29-77-G-0100 and the National Science Foundation under Grant no. DMR-76-02733.

References

1. D. G. RICKERBY, B. N. PRAMILA BAI and N. H. MACMILLAN, *J. Mater. Sci.* 14 (1979).
2. *Idem*, Basic Mechanisms of Erosion in Ceramics, in "Proceedings of the Fourth International Meeting on Modern Ceramic Technologies", Saint-Vincent, Italy, May (1979).

3. D. G. RICKERBY and N. H. MACMILLAN, Mechanisms of Solid Particle Erosion in Crystalline Materials, in "Proceedings of the Fifth International Conference on Erosion by Solid and Liquid Impact", Cambridge, England, September (1979).
4. K. L. JOHNSON, J. J. O'CONNOR and A. C. WOODWARD, *Proc. Roy. Soc.* **A334** (1973) 95.
5. B. LAWN and R. WILSHAW, *J. Mater. Sci.* **10** (1975) 1049.

Received 4 April
and accepted 11 May 1979

D. G. RICKERBY
B. N. PRAMILA BAI
N. H. MACMILLAN
Materials Research Laboratory,
The Pennsylvania State University,
University Park,
Pennsylvania 16802,
USA

The central region of the calcium oxide–gallium oxide system

During attempts to grow single crystal calcium gallate ($CaGa_2O_4$) from the melt using the Czochralski technique, it became necessary to check the phase diagram in the region of the compound, $CaGa_2O_4$ since different authors have variously assigned to this mole ratio, no compound [1], two compounds [2], and three compounds [3], nominally all with the formula $CaGa_2O_4$. This communication describes investigations on this system and attempts to rationalize the results obtained and those already published.

Mixtures of calcium carbonate and gallium oxide of the highest commercially available quality, with a total metallic impurity content about 10 ppm, were made in the range 35 to 65 mol% Ga_2O_3, sixteen mixtures in all. Each sample was subsequently placed in a differential thermal analysis (DTA) unit heated until molten and then cooled. The temperature was then recycled and a DTA trace obtained, the heating and cooling rate being $10^\circ C\,min^{-1}$. The samples

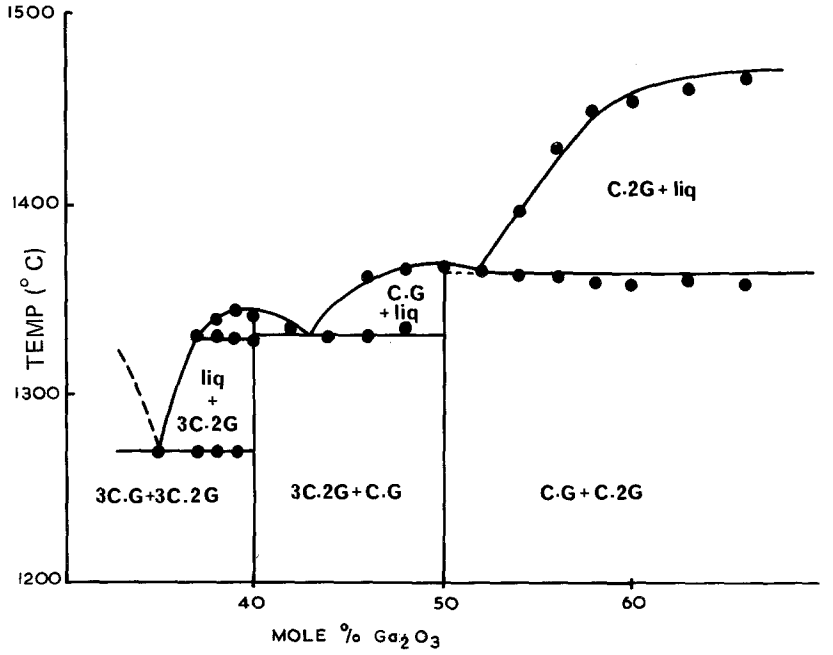

Figure 1 The $CaO–Ga_2O_3$ system. C = CaO, G = Ga_2O_3. Eutectic between 3C.G and 3C.2G at 35 mol% Ga_2O_3 1270 ± 3° C. Maximum melting point 35 to 45 mol% 1345 ± 3° C. Eutectic between 3C.2G and C.G at 43 mol% Ga_2O_3 1332 ± 3° C. Melting point 50 mol% mixture 1368 ± 3° C.

0022–2461/79/123008–03$02.30/0